Large Spin-Wave Bullet in a Ferrimagnetic Insulator Driven by the Spin Hall Effect

M. B. Jungfleisch,[1,*] W. Zhang,[1] J. Sklenar,[1,2] J. Ding,[1] W. Jiang,[1] H. Chang,[3] F. Y. Fradin,[1] J. E. Pearson,[1] J. B. Ketterson,[2] V. Novosad,[1] M. Wu,[3] and A. Hoffmann[1]

[1]*Materials Science Division, Argonne National Laboratory, Argonne, Illinois 60439, USA*
[2]*Department of Physics and Astronomy, Northwestern University, Evanston, Illinois 60208, USA*
[3]*Department of Physics, Colorado State University, Fort Collins, Colorado 80523, USA*

(Received 28 July 2015; revised manuscript received 26 October 2015; published 1 February 2016)

Because of its transverse nature, spin Hall effects (SHE) provide the possibility to excite and detect spin currents and magnetization dynamics even in magnetic insulators. Magnetic insulators are outstanding materials for the investigation of nonlinear phenomena and for novel low power spintronics applications because of their extremely low Gilbert damping. Here, we report on the direct imaging of electrically driven spin-torque ferromagnetic resonance (ST-FMR) in the ferrimagnetic insulator $Y_3Fe_5O_{12}$ based on the excitation and detection by SHEs. The driven spin dynamics in $Y_3Fe_5O_{12}$ is directly imaged by spatially resolved microfocused Brillouin light scattering spectroscopy. Previously, ST-FMR experiments assumed a uniform precession across the sample, which is not valid in our measurements. A strong spin-wave localization in the center of the sample is observed indicating the formation of a nonlinear, self-localized spin-wave "bullet".

DOI: 10.1103/PhysRevLett.116.057601

Magnetic memory and logic devices rely on the efficient manipulation of the orientation of their magnetization using low power [1–3]. Recently, there has been revitalized interest in the ferrimagnetic insulator yttrium iron garnet (YIG, $Y_3Fe_5O_{12}$) motivated by the discovery of spintronic effects by combining this material and heavy metals such as Pt [4–9]. Its extremely small magnetic damping enables low power data transmission and processing on the basis of magnons, the elementary quanta of magnetic excitations. [4–6,10–14]. In addition, the low damping YIG also enables nonlinear phenomena where the superposition principle breaks down [13]. Previous work reported on the formation of spin-wave caustics [15], spatiotemporal self-focusing of spin waves [16], Bose Einstein condensation of magnons [17], and nonlinear mode conversion [18] to name only a few. Recently, it has become possible to grow nanometer-thick YIG films, which allow the preparation of micro- and nanostructured devices [6,10,11,14,19,20]. Therefore, the study of nonlinear spin dynamics in miniaturized YIG systems has only just begun.

Independent of the progress of the YIG film growth, the development in employing spin-orbit interaction in heavy metals [21,22] and their alloys [23] in contact with a ferromagnet (FM) has flourished. The spin Hall effects (SHE) [24,25] can be used for the generation of strong current-driven torques on the magnetization in the FM layer. The resultant spin current can drive spin-torque ferromagnetic resonance (ST-FMR) in bilayers consisting of ferromagnetic and nonmagnetic metals and can be detected by a homodyne mixing of the microwave signal with the anisotropic magnetoresistance [26]. Recent theories propose that ST-FMR can be extended to insulating FM or normal metal bilayers. Here, the detection of magnetization precession occurs by spin pumping and a rectification of the spin Hall magnetoresistance [27,28]. We recently showed that this rectification process is, indeed, possible in YIG/Pt bilayers [29]. All previous analysis of electric measurements assume uniform precession across the sample [26,30]. In order to validate this assumption, it is highly desirable to image ac current-driven spin dynamics spatially resolved and frequency resolved. These investigations provide interesting insights in the underlying physics, such as whether bulk or edge modes are preferably excited by ST-FMR or nonlinear spin dynamics may occur.

In this Letter, we show, experimentally, the excitation of spin dynamics in microstructured magnetic insulators by the SHE of an adjacent heavy metal and observe the formation of a nonlinear, self-localized spin-wave intensity in the center of the sample [31–33]. The magnetization dynamics in a nanometer-thick YIG layer is driven simultaneously by the Oersted field and a spin torque originating from a spin current generated by the SHE of an attached Pt layer. The dynamics is detected in two complementary ways: (1) Electrically, by a rectification mechanism of the spin Hall magnetoresistance (SMR) [34–36] as well as by spin pumping [4–6,37–39], and (2) optically, by spatially resolved Brillouin light scattering (BLS) microscopy [40]. The experimental findings are further validated by micromagnetic simulations [41].

YIG(40 nm)/Pt bilayers were fabricated by *in situ* magnetron sputtering under high-purity argon atmosphere on single crystal gadolinium gallium garnet ($Gd_3Ga_5O_{12}$) substrates of 500 μm thickness with (111) orientation [19]. For the electrical measurements, a Pt thickness of 2 nm was used, while for the optical investigations the thickness was 5 nm in order to minimize the influence of additional

heating effects by the laser. In a subsequent fabrication process, stripes in the shape of $30 \times 5\ \mu m^2$ (electrical measurements) and $5 \times 5\ \mu m^2$ (optical measurements) were patterned by photolithography and ion milling [6]. A coplanar waveguide made of Ti/Au (3 nm/120 nm) was structured on top of the bar allowing the signal line to serve as a lead for the YIG/Pt bar as illustrated in Fig. 1(a). In this ST-FMR configuration, a bias T is utilized to allow for simultaneous transmission of a microwave signal with dc voltage detection via lock-in technique across the Pt. For this purpose, the amplitude of the rf current is modulated at 3 kHz. We use a BLS microscope with a spatial resolution of 250 nm, where the laser spot is focused onto the sample and the frequency shift of the back reflected light is analyzed by a multipass tandem Fabry Pérot interferometer [40]. The detected BLS intensity is proportional to the square of the dynamic magnetization, i.e., the spin-wave intensity.

In order to excite a dynamic response by ST-FMR in the YIG system, a rf signal is passed through the Pt layer. The magnetization dynamics is governed by a modified Landau-Lifshitz-Gilbert equation [27,28]

$$\frac{d\mathbf{M}}{dt} = -|\gamma|\mathbf{M} \times \mathbf{H}_{\text{eff}} + \alpha \mathbf{M} \times \frac{d\mathbf{M}}{dt} + \frac{|\gamma|\hbar}{2eM_s d_F}\mathbf{J}_s, \quad (1)$$

where γ is the gyromagnetic ratio, $\mathbf{H}_{\text{eff}} = \mathbf{h}_{\text{rf}} + \mathbf{H}_D + \mathbf{H}$ is the effective magnetic field including the microwave magnetic field $\mathbf{h}_{\text{rf}}$, demagnetization fields $\mathbf{H}_D$, and the bias magnetic field $\mathbf{H}$. α is the Gilbert damping parameter [the second term describes the damping torque τ_α, Fig. 1(b)] and $\mathbf{J}_s$ is a transverse spin current at the interface generated by the SHE from the alternating charge current in the Pt layer and spin pumping from the YIG layer [27,28]

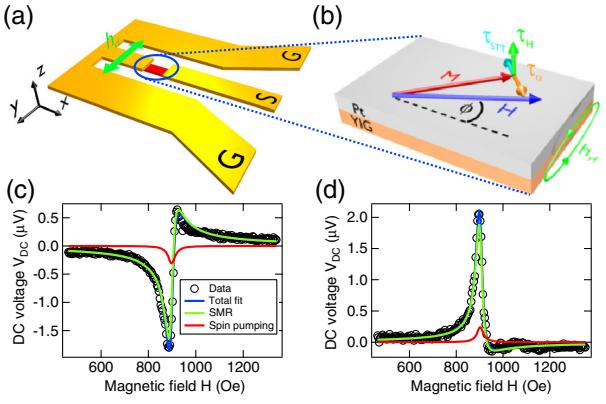

FIG. 1. (a) Schematic of the ST-FMR experimental setup (b) ST-FMR mechanism in the YIG/Pt bilayer. The alternating rf current drives an Oersted field h_{rf} exerting a fieldlike torque τ_{H} on the magnetization $\mathbf{M}$. At the same time a oscillatory transverse spin accumulation at the YIG/Pt interface is generated by the SHE which results in a dampinglike torque τ_{STT}. (c) and (d) Typical dc voltage spectra recorded at in-plane angles of $\phi = 30°$ and $\phi = 240°$ and $P = +10$ dBm.

$$\mathbf{J}_s = \frac{\text{Re}(g_{\text{eff}}^{\uparrow\downarrow})}{e}\mathbf{M} \times (\mathbf{M} \times \mu_s) + \frac{\text{Im}(g_{\text{eff}}^{\uparrow\downarrow})}{e}\mathbf{M} \times \mu_s + \frac{\hbar}{e}[\text{Re}(g_{\text{eff}}^{\uparrow\downarrow})\mathbf{M} \times \partial_t \mathbf{M} + \text{Im}(g_{\text{eff}}^{\uparrow\downarrow})\partial_t \mathbf{M}]. \quad (2)$$

Here, $g_{\text{eff}}^{\uparrow\downarrow}$ is the effective spin-mixing conductance and μ_s is the spin accumulation at the YIG/Pt interface. The first term in Eq. (2) describes an antidampinglike torque τ_{STT} and the second term is a fieldlike torque τ_H. The last two terms describe the spin pumping contribution. As illustrated in Fig. 1(b) and described by Eq. (1), the magnetization is driven by the independent torque terms containing h_{rf} and J_s.

First, we describe the electrical characterization of the YIG/Pt bars by means of ST-FMR. Figures 1(c) and 1(d) illustrate typical dc voltage spectra; exemplarily, we show spectra recorded at in-plane angles of $\phi = 30°$ and $\phi = 240°$, with applied rf power $P = +10$ dBm. A signal is observed when the system is driven resonantly. The data are analyzed using the model proposed by Chiba *et al.* [27,28,42]. According to the model, two signals contribute to the dc voltage: (1) spin pumping which manifests in a symmetric contribution to the Lorentzian line shape; (2) spin Hall magnetoresistance which is a superimposed symmetric and antisymmetric Lorentzian curve [Figs. 1(c) and 1(d)].

Figure 2(a) illustrates dc voltage spectra at a fixed microwave frequency $f = 4$ GHz for three different applied powers. The offset is due to the longitudinal spin Seebeck effect (SSE) [8,9] occurring off resonance [42]. The inset in Fig. 2(a) shows the resonance peak at $P = +15$ dBm. Clearly, a less intense, secondary mode in addition to the main mode is detected. According to the Chiba model [27,28], the dc voltage signal can be deconvoluted into a spin-pumping and a SMR contribution as also shown in Figs. 1(c) and 1(d). To analyze the data employing the model, we use a spin-mixing conductance of $g_{\text{eff}}^{\uparrow\downarrow} = 3.36 \times 10^{14}\ \Omega^{-1}\,\text{m}^{-2}$ and a spin-Hall angle of $\gamma_{\text{SHE}} = 0.09$ [47]. We added to Chiba's model a phenomenological $\sin\phi$ term to the in-plane angular dependence of the symmetric component of the line shape. This term is consistent with an on-resonant heating leading to SSE rectification. For the fit illustrated in Figs. 1(c) and 1(d), we removed the SSE contribution from the symmetric component of the line shape [29] and analyzed the data using Chiba's original model with a phase difference of $\delta = -51° \pm 6°$ such that the spin-mixing conductance was real. Alternatively, it is possible to assume a zero phase shift and a nonzero imaginary spin-mixing conductance to describe the data [29]. Figures 2(b) and 2(c) show the angular dependences of the symmetric, V_S, and antisymmetric, V_{AS}, portion to the dc voltage V_{dc}. The model predicts the same angular dependent behavior $\propto \sin 2\phi \cos\phi$ for V_S and V_{AS}. We observe an additional $\sin\phi$ dependence to V_S that comes from the SSE. As seen in Figs. 2(b) and 2(c), we find a good agreement between theory (solid lines) and experiment for both curves.

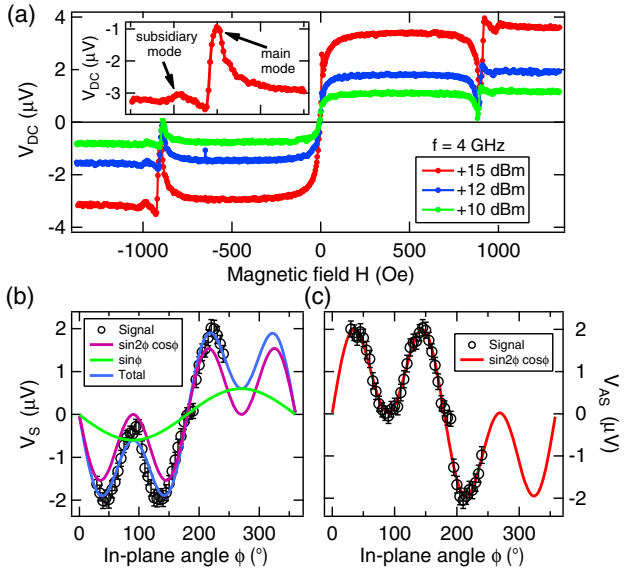

FIG. 2. (a) Typical V_{DC} spectra at a constant frequency $f = 4$ GHz for various applied microwave powers. The inset shows the resonance peak at $P = +15$ dBm. Two modes are detected. (b) In-plane angular dependence of the symmetric portion to V_{DC}. The purple curve is the $\sin 2\phi \cos\phi$ dependence from the ST-FMR model we use. The green curve shows an additional $\sin\phi$ dependence in resonance. The sum of both signals is shown as blue curve. (c) Antisymmetric portion to V_{DC} as a function of the in-plane angle following the expected $\sin 2\phi \cos\phi$ dependence.

In the following, we compare the electrical measurements with the results obtained by BLS imaging. The optical measurements were performed on YIG(40 nm)/Pt(5 nm) bars having a lateral size of 5×5 μm^2. The external magnetic field is applied at an angle of $\phi \sim 45°$ where the dc voltage detection is maximized [Fig. 2(b)] and the probing BLS laser beam is focused onto the center of the sample. Figure 3 shows the resonance frequency as a function of the bias magnetic field measured by BLS in a false color-coded image where red indicates a high spin-wave intensity, and the blue area shows the absence of spin waves. The measured frequency-field dependence is in agreement with the electrical measurements as shown in the inset: As the field increases, the resonance shifts to higher frequencies as is expected from the Kittel equation, $f = (|\gamma|/2\pi)\sqrt{H(H + 4\pi M_{\text{eff}})}$, where M_{eff} is the effective magnetization.

As is apparent from Fig. 2(a) and Fig. 3, magnetization dynamics can be excited in a certain bandwidth around the resonance which is determined by the specific device characteristics. Furthermore, both figures (electrical and optical detection) suggest that there is an additional mode below the main mode. At first, one might identify this mode as an edge mode [48,49]. However, this is not the case as will be discussed below.

In order to spatially map the spin-wave intensity, the applied magnetic field is kept fixed at $H = 665$ Oe.

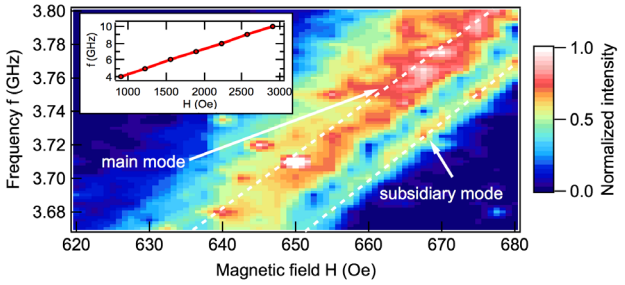

FIG. 3. Resonance frequency as a function of bias magnetic field measured by BLS illustrated in a color-coded image. The laser spot was focused onto the center of the sample while the rf frequency and magnetic field were varied. As for the electrical measurements two modes are detected by BLS. The inset shows corresponding field dependence of the resonance measured by electrical means.

Figure 4 illustrates the experimental observations in false color-coded images. At an excitation frequency below the resonance frequency, e.g., $f = 3.7$ GHz, no magnetization dynamics is detected [Fig. 4(a)]. As the frequency increases, the system is driven resonantly and a strong spin-wave intensity is observed from $f = 3.725$ GHz to $f = 3.8$ GHz, Figs. 4(b) and 4(c). Increasing the frequency even further results in a diminished signal, Fig. 4(d) for $f = 3.85$ GHz. At even larger frequencies no magnetization dynamics is detected as it is also apparent from Fig. 3. In conventional electrical ST-FMR measurements, a uniform spin-wave intensity distribution across the lateral sample dimensions is assumed. However, as our experimental results show, this assumption is not fulfilled: A strong spin-wave signal is localized in the center of the YIG/Pt bar. It is desirable to experimentally investigate at what minimum excitation power the formation of the

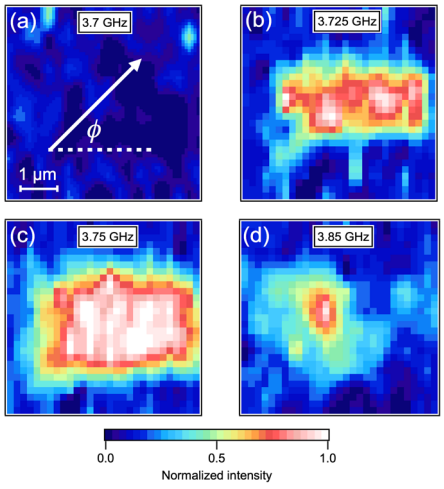

FIG. 4. Spatially-resolved BLS map of the 5×5 μm^2 large YIG/Pt sample. The magnetic field $H = 665$ Oe is applied at $\phi \sim 45°$. (a)—(d) Driving microwave frequency increases from 3.7 GHz to 3.85 GHz, microwave power $P = +17$ dBm.

localization occurs. However, in the investigated range of powers we always observe a localization in the center of the sample [42]. For rf powers of less than +11 dBm, the BLS signal is below our noise floor.

In spite of this experimental limitation, we also carried out micromagnetic simulations in order to gain further insight into the underlying magnetization dynamics. The simulations qualitatively confirmed the experimental observations as is depicted in Fig. 5: Two modes can be identified in the simulations, Fig. 5(a). In the low power regime, which is not accessible experimentally, we find that the spatial magnetization distribution of the main mode is almost uniform and the less intense subsidiary mode is localized at the edges ($h_{\mathrm{rf}} = 0.25$ Oe, not shown). With increasing rf power, the spatial distributions of both modes transform and at a threshold of $h_{\mathrm{rf}} \approx 1$ Oe a localization of both modes in the center of the sample is observed. Figures 5(b) and 5(c) show the corresponding spatial dynamic magnetization distributions at $h_{\mathrm{rf}} = 5$ Oe and agree well with the experimental findings, Fig. 4.

This spatial profile can be understood as the formation of a nonlinear, self-localized "bulletlike" spin-wave intensity [16] caused by nonlinear cross coupling between eigenmodes in the system [18]. This process is mainly

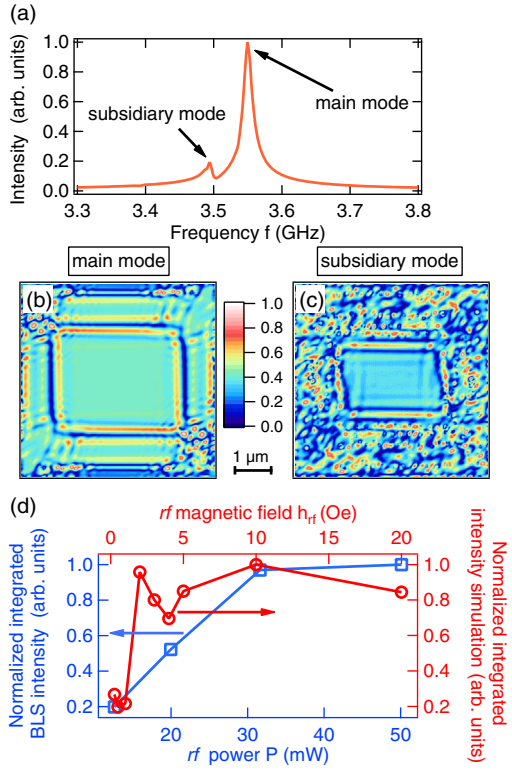

FIG. 5. Micromagnetic simulations: (a) The spectrum reveals two modes. Spatially-resolved magnetization distribution of the main mode, (b), and the less intense, subsidiary mode, (c). (d) The normalized integrated BLS intensity saturates at high excitation powers P, which is validated by micromagnetic simulations at large driving rf magnetic fields h_{rf}.

determined by nonlinear spin-wave damping which transfers energy from the initially excited ferromagnetic resonance into other spin-wave modes rather than into the crystalline lattice [18]. To check this assumption, we plotted, in Fig. 5(d), the normalized integrated BLS intensity as well as the integrated spatial magnetization distribution as a function of the applied microwave power and the rf magnetic field, respectively. Both integrated signals demonstrate a nonlinear behavior and saturate at high powers or microwave magnetic fields. This observation is a direct manifestation of nonlinear damping: Energy is absorbed by the ferromagnetic resonance and redistributed to secondary spin-wave modes more and more effectively [18]. Self-focusing of spin-wave bullets was first observed in macroscopic micrometer-thick YIG samples where dynamics was driven by conventional microwave techniques [16]. In contrast to those previous studies, here, we show that this phenomenon can (1) also be observed in microstructured YIG samples and (2) be excited by ST-FMR.

Until now, ST-FMR experiments assumed a uniform magnetization precession [26–28,30]. However, as our spatially resolved BLS results demonstrate and micromagnetic simulations confirm, the driven lateral spin-wave intensity distribution in insulating FMs deviates from this simple model at higher excitation powers which are common in ST-FMR measurements. The formation of a localized spin-wave mode was not considered in previous ST-FMR experiments either in metals or in insulators. Our findings have direct consequences on the analysis and interpretation of ST-FMR experiments. The precession amplitude is not uniform across the sample, implying that the effective spin-mixing conductance $g_{\mathrm{eff}}^{\uparrow\downarrow}$ is actually an average over the sample cross section. In areas where the precession amplitude is large, $g_{\mathrm{eff}}^{\uparrow\downarrow}$ is underestimated, whereas it is overestimated in low-intensity areas. This also complicates the determination of the spin-Hall angle from ST-FMR measurements.

Micromagnetic simulations show phase inhomogeneity, specifically around the perimeter of the mode. The phase inhomogeneity tends to equally lag and lead the main uniform phase of the center mode; effectively, the phase inhomogeneity then leads to no significant change to the line shape. However, assuming the phase at the perimeter to be uniformly leading, the bulk phase results in a correction to the line shape that is still negligible because the effective area and amplitude where the phase is deviating is significantly smaller than the bulk area. Nevertheless, in general, the issue of inhomogeneous phase distribution may complicate the analysis of electrical ST-FMR spectra, especially in smaller samples.

In conclusion, we demonstrated that the concept of ST-FMR can be extended to magnetic insulators where the formation of a nonlinear, self-localized spin-wave intensity driven by an alternating current was observed. We adopted an electrically driven ST-FMR excitation and detection

scheme in magnetic insulator, (YIG)/heavy normal metal (Pt) bilayers, that was originally developed for all-metallic systems. A dc voltage in YIG/Pt bilayers was observed under resonance condition by a SMR-mediated spin-torque diode effect in agreement with theoretical predictions. Spatially resolved BLS microscopy revealed a strong bulletlike spin-wave localization in the center of the sample due to nonlinear cross coupling of eigenmodes in the system. Since the observed electrical signal is sufficiently large and the signal-to-noise ratio is reasonably good, down-scaling of sample dimensions to the nanometer scale is feasible.

We thank Stephen Wu for assistance with ion milling. The work at Argonne, including sample fabrication, microwave measurements, and BLS imaging, was supported by the U.S. Department of Energy, Office of Science, Materials Science and Engineering Division. Lithography was carried out at the Center for Nanoscale Materials, an Office of Science user facility, which is supported by the U.S. DOE, Office of Science, Basic Energy Science under Contract No. DE-AC02-06CH11357. The work at Colorado State University preparing the YIG films was supported by the U.S. Army Research Office (Grant No. W911NF-14-1-0501), the U.S. National Science Foundation (Grant No. ECCS-1231598), C-SPIN (one of the SRC STARnet Centers sponsored by MARCO and DARPA), and the U.S. Department of Energy (Grant No. DE-SC0012670).

*jungfleisch@anl.gov

[1] D. C. Ralph and M. D. Stiles, J. Magn. Magn. Mater. **320**, 1190 (2008).
[2] A. Hoffmann and H. Schultheiß, Curr. Opin. Solid State Mater. Sci. **19**, 253 (2015).
[3] A. Hoffmann and S. D. Bader, Phys. Rev. Applied **4**, 047001 (2015).
[4] Y. Kajiwara, K. Harii, S. Takahashi, J. Ohe, K. Uchida, M. Mizuguchi, H. Umezawa, H. Kawai, K. Ando, K. Takanashi, S. Maekawa, and E. Saitoh, Nature (London) **464**, 262 (2010).
[5] M. B. Jungfleisch, A. V. Chumak, V. I. Vasyuchka, A. A. Serga, B. Obry, H. Schultheiss, P. A. Beck, A. D. Karenowska, E. Saitoh, and B. Hillebrands, Appl. Phys. Lett. **99**, 182512 (2011).
[6] M. B. Jungfleisch, W. Zhang, W. Jiang, H. Chang, J. Sklenar, S. M. Wu, J. E. Pearson, A. Bhattacharya, J. B. Ketterson, M. Wu, and A. Hoffmann, J. Appl. Phys. **117**, 17D128 (2015).
[7] Y. Sun, H. Chang, M. Kabatek, Y.-Y. Song, Z. Wang, M. Jantz, W. Schneider, M. Wu, E. Montoya, B. Kardasz, B. Heinrich, S. G. E. te Velthuis, H. Schultheiss, and A. Hoffmann, Phys. Rev. Lett. **111**, 106601 (2013).
[8] K. Uchida, S. Takahashi, K. Harii, J. Ieda, W. Koshibae, K. Ando, S. Maekawa, and E. Saitoh, Nature (London) **455**, 778 (2008).
[9] M. B. Jungfleisch, T. An, K. Ando, Y. Kajiwara, K. Uchida, V. I. Vasyuchka, A. V. Chumak, A. A. Serga, E. Saitoh, and B. Hillebrands, Appl. Phys. Lett. **102**, 062417 (2013).
[10] A. Hamadeh, O. d'Allivy Kelly, C. Hahn, H. Meley, R. Bernard, A. H. Molpeceres, V. V. Naletov, M. Viret, A. Anane, V. Cros, S. O. Demokritov, J. L. Prieto, M. Muñoz, G. de Loubens, and O. Klein, Phys. Rev. Lett. **113**, 197203 (2014).
[11] O. d'Allivy Kelly, A. Anane, R. Bernard, J. Ben Youssef, C. Hahn, A. H. Molpeceres, C. Carrétéro, E. Jacquet, C. Deranlot, P. Bortolotti, R. Lebourgeois, J.-C. Mage, G. de Loubens, O. Klein, V. Cros, and A. Fert, Appl. Phys. Lett. **103**, 082408 (2013).
[12] M. Wu and A. Hoffmann, *Recent advances in magnetic insulators—From spintronics to microwave applications*, Solid State Physics Vol. 64 (Academic Press, Amsterdam, 2013).
[13] A. G. Gurevich and G. A. Melkov, *Magnetization oscillations and waves*, (CRC Press, Boca Raton, FL, 1996).
[14] P. Pirro, T. Brächer, A. V. Chumak, B. Lägel, C. Dubs, O. Surzhenko, P. Görnert, B. Leven, and B. Hillebrands, Appl. Phys. Lett. **104**, 012402 (2014).
[15] T. Schneider, A. A. Serga, A. V. Chumak, C. W. Sandweg, S. Trudel, S. Wolff, M. P. Kostylev, V. S. Tiberkevich, A. N. Slavin, and B. Hillebrands, Phys. Rev. Lett. **104**, 197203 (2010).
[16] M. Bauer, O. Büttner, S. O. Demokritov, B. Hillebrands, V. Grimalsky, Yu. Rapoport, and A. N. Slavin, Phys. Rev. Lett. **81**, 3769 (1998).
[17] S. O. Demokritov, V. E. Demidov, O. Dzyapko, G. A. Melkov, A. A. Serga, B. Hillebrands, and A. N. Slavin, Nature (London) **443**, 430 (2006).
[18] M. Kostylev, V. E. Demidov, U.-H. Hansen, and S. O. Demokritov, Phys. Rev. B **76**, 224414 (2007).
[19] H. Chang, P. Li, W. Zhang, T. Liu, A. Hoffmann, L. Deng, and M. Wu, IEEE Magn. Lett. **5**, 6700104 (2014).
[20] S. Li, W. Zhang, J. Ding, J. E. Pearson, V. Novosad, and A. Hoffmann, Nanoscale **8**, 388 (2016).
[21] A. Hoffmann, IEEE Trans. Magn. **49**, 5172 (2013).
[22] W. Zhang, M. B. Jungfleisch, W. Jiang, J. Sklenar, F. Y. Fradin, J. E. Pearson, J. B. Ketterson, and A. Hoffmann, J. Appl. Phys. **117**, 172610 (2015).
[23] W. Zhang, M. B. Jungfleisch, W. Jiang, J. E. Pearson, A. Hoffmann, F. Freimuth, and Y. Mokrousov, Phys. Rev. Lett. **113**, 196602 (2014).
[24] M. I. D'yakonov and V. I. Perel', Sov. Phys. JETP Lett. **13**, 467 (1971).
[25] J. E. Hirsch, Phys. Rev. Lett. **83**, 1834 (1999).
[26] L. Liu, T. Moriyama, D. C. Ralph, and R. A. Buhrman, Phys. Rev. Lett. **106**, 036601 (2011).
[27] T. Chiba, G. E. W. Bauer, and S. Takahashi, Phys. Rev. Applied **2**, 034003 (2014).
[28] T. Chiba, M. Schreier, G. E. W. Bauer, and S. Takahashi, J. Appl. Phys. **117**, 17C715 (2015).
[29] J. Sklenar, W. Zhang, M. B. Jungfleisch, W. Jiang, H. Chang, J. E. Pearson, M. Wu, J. B. Ketterson, and A. Hoffmann, Phys. Rev. B **92**, 174406 (2015).
[30] A. R. Mellnik, J. S. Lee, A. Richardella, J. L. Grab, P. J. Mintun, M. H. Fischer, A. Vaezi, A. Manchon, E.-A. Kim, N. Samarth, and D. C. Ralph, Nature (London) **511**, 449 (2014).
[31] V. E. Demidov, S. Urazhdin, H. Ulrichs, V. Tiberkevich, A. Slavin, D. Baither, G. Schmitz, and S. O. Demokritov, Nat. Mater. **11**, 1028 (2012).
[32] A. Slavin and V. Tiberkevich, Phys. Rev. Lett. **95**, 237201 (2005).

[33] R. H. Liu, W. L. Lim, and S. Urazhdin, Phys. Rev. Lett. **110**, 147601 (2013).
[34] J. C. Sankey, P. M. Braganca, A. G. F. Garcia, I. N. Krivorotov, R. A. Buhrman, and D. C. Ralph, Phys. Rev. Lett. **96**, 227601 (2006).
[35] H. Nakayama, M. Althammer, Y.-T. Chen, K. Uchida, Y. Kajiwara, D. Kikuchi, T. Ohtani, S. Geprägs, M. Opel, S. Takahashi, R. Gross, G. E. W. Bauer, S. T. B. Goennenwein, and E. Saitoh, Phys. Rev. Lett. **110**, 206601 (2013).
[36] M. Schreier, T. Chiba, A. Niedermayr, J. Lotze, H. Huebl, S. Geprägs, S. Takahashi, G. E. W. Bauer, R. Gross, and S. T. B. Goennenwein, Phys. Rev. B **92**, 144411 (2015).
[37] Y. Tserkovnyak, A. Brataas, and G. E. W. Bauer, Phys. Rev. Lett. **88**, 117601 (2002).
[38] A. Azevedo, L. H. Vilela Leão, R. L. Rodríguez-Suárez, A. B. Oliveira, and S. M. Rezende, J. Appl. Phys. **97**, 10C715 (2005).
[39] O. Mosendz, J. E. Pearson, F. Y. Fradin, G. E. W. Bauer, S. D. Bader, and A. Hoffmann, Phys. Rev. Lett. **104**, 046601 (2010).
[40] B. Hillebrands, in *Novel Techniques for Characterizing Magnetic Materials*, edited by Y. Zhu (Springer, New York, 2005).
[41] A. Vansteenkiste, J. Leliaert, M. Dvornik, M. Helsen, F. Garcia-Sanchez, and B. Van Waeyenberge, AIP Adv. **4**, 107133 (2014).
[42] See Supplemental Material at http://link.aps.org/supplemental/10.1103/PhysRevLett.116.057601 for further information on the micromagnetic simulations, the line shape analysis, the spin Seebeck contribution to the signal and power-dependent BLS measurements, which includes Refs. [43–46].
[43] J. P. Park, P. Eames, D. M. Engebretson, J. Berezovsky, and P. A. Crowell, Phys. Rev. Lett. **89**, 277201 (2002).
[44] M. Buess, R. Höllinger, T. Haug, K. Perzlmaier, U. Krey, D. Pescia, M. R. Scheinfein, D. Weiss, and C. H. Back, Phys. Rev. Lett. **93**, 077207 (2004).
[45] R. D. McMichael and M. D. Stiles, J. Appl. Phys. **97**, 10J901 (2005).
[46] M. Agrawal, A. A. Serga, V. Lauer, E. Th. Papaioannou, B. Hillebrands, and V. I. Vasyuchka, Appl. Phys. Lett. **105**, 092404 (2014).
[47] W. Zhang, V. Vlaminck, J. E. Pearson, R. Divan, S. D. Bader, and A. Hoffmann, Appl. Phys. Lett. **103**, 242414 (2013).
[48] J. Jorzick, S. O. Demokritov, B. Hillebrands, M. Bailleul, C. Fermon, K. Y. Guslienko, A. N. Slavin, D. V. Berkov, and N. L. Gorn, Phys. Rev. Lett. **88**, 047204 (2002).
[49] S. Neusser and D. Grundler, Adv. Mater. **21**, 2927 (2009).